

# Quantum Criticality in doped $\text{CePd}_{1-x}\text{Rh}_x$ Ferromagnet

J.G. Sereni<sup>1</sup>, T. Westerkamp<sup>2</sup>, R. KÜchler<sup>2</sup>, N. Caroca-Canales<sup>2</sup>, P. Gegenwart<sup>2</sup>, C. Geibel<sup>2</sup>

<sup>1</sup> *Lab. Bajas Temperaturas, Centro Atómico Bariloche, 8400 S.C. Bariloche, Argentina*

<sup>2</sup> *Max-Planck Institute for Chemical Physics of Solids, D-01187 Dresden, Germany*

(Dated: October 22, 2018)

$\text{CePd}_{1-x}\text{Rh}_x$  alloys exhibit a continuous evolution from ferromagnetism ( $T_C = 6.5$  K) at  $x = 0$  to a mixed valence (MV) state at  $x = 1$ . We have performed a detailed investigation on the suppression of the ferromagnetic (F) phase in this alloy using dc- ( $\chi_{dc}$ ) and ac-susceptibility ( $\chi_{ac}$ ), specific heat ( $C_m$ ), resistivity ( $\rho$ ) and thermal expansion ( $\beta$ ) techniques. Our results show a continuous decrease of  $T_C(x)$  with negative curvature down to  $T_C = 3$  K at  $x^* = 0.65$ , where a positive curvature takes over. Beyond  $x^*$ , a cusp in  $\chi_{ac}$  is traced down to  $T_C^* = 25$  mK at  $x = 0.87$ , locating the critical concentration between  $x = 0.87$  and  $0.90$ . The quantum criticality of this region is recognized by the  $-\log(T/T_0)$  dependence of  $C_m/T$ , which transforms into a  $T^{-q}$  ( $q \approx 0.5$ ) one at  $x = 0.87$ . At high temperature, this system shows the onset of valence instability revealed by a deviation from Vegard's law (at  $x_V \approx 0.75$ ) and increasing hybridization effects on high temperature  $\chi_{dc}$  and  $\rho(T)$ . Coincidentally, a Fermi liquid contribution to the specific heat arises from the MV component, which becomes dominant at the CeRh limit. In contrast to antiferromagnetic systems, no  $C_m/T$  flattening is observed for  $x > x_{cr}$  rather the mentioned power law divergence, which coincides with a change of sign of  $\beta(T)$ . The coexistence of F and MV components and the sudden changes in the  $T$  dependencies are discussed in the context of randomly distributed magnetic and Kondo couplings.

PACS numbers: Pacs: 71.27.+a, 75.30.-m, 75.40.Cx, 75.50.Cc

## I. INTRODUCTION

The physics related to magnetic critical points at very low temperature, where quantum fluctuations compete with classical thermal fluctuations, is a topic of increasing attraction. The wealthy spectrum of recently discovered new properties has triggered intense experimental and theoretical activity, involving a large number of magnetic phase diagrams.[1] The magnetic phase boundaries of those systems are tuned to different classes of critical points,[2, 3] where the long range order is suppressed by applying pressure or alloying. Since most of the current investigations are devoted to antiferromagnetic (AF) systems, suitable candidates for the study of ferromagnetic (F) systems remain scarce.[4] Not only the number of available exemplary AF or F systems makes the difference between them, rather intrinsic physical properties like those observed in  $3d$  compounds [5] or the proposed by theoretical models.[6] However, up to date the great amount of AF systems exhibiting coexistence of magnetic order and Kondo effect with respect to the number of F ones remains a puzzling problem. This asymmetry cannot be simply explained by a distribution of  $Ce - Ce$  spacings in their respective lattices, where inter-site magnetic interactions ( $J_R$ ) act mediated by the RKKY mechanism. In spite of that, it is observed that F Ce binary compounds only appear within a narrow  $Ce - Ce$  spacing range:  $3.7 < d_{Ce-Ce} < 4.1 \text{ \AA}$ . [7] Furthermore, in coincidence with the fact that Kondo effect is related to an AF spin-electron-coupling parameter ( $J_K$ ), none of the known F Ce compounds show conclusive indications of significant hybridization effects, which even excludes heavy fermion behavior. Consequently, the F- order is generally taken as hallmark of trivalent  $\text{Ce}^{3+}$  ground state [4, 7] when it reaches the expected entropy ( $S_m = R \ln 2$ ) at  $T \approx T_C$ .

The few known F Ce phase diagrams studied as a function of pressure ( $p$ ) as control parameter on Ce-binary compounds also show some peculiarities. For example, no superconductivity was detected under pressure, whereas the  $T_C(p)$  phase boundary show the characteristic maximum described by Doniach-Lavagna model.[8] Under alloying, other intrinsic differences between F and AF systems are observed concerning their respective "final" (non-magnetic) ground states (GS). Whereas the former systematically exhibit a *mixed-valence* (MV) state, the latter show *heavy-fermion* (HF) behavior.[9] Such a difference indicates that a strong hybridization (even including charge fluctuations) is required to overcome a F-GS, whereas in AF spin fluctuations (with  $T_K \simeq 10$  K) are enough to screen Ce magnetic moments.[9, 10] Concerning ternary compounds like  $\text{CeRu}_2\text{Ge}_2$  [11] and  $\text{CePd}_2\text{Al}_2\text{Ga}$ , [12] both undergo a transition to AF phases before to reach the critical pressure.

The distinctive features between F- and AF-systems suggest intrinsic differences in their critical points. In fact, theory predicts that magnetic, thermal and transport properties differ between

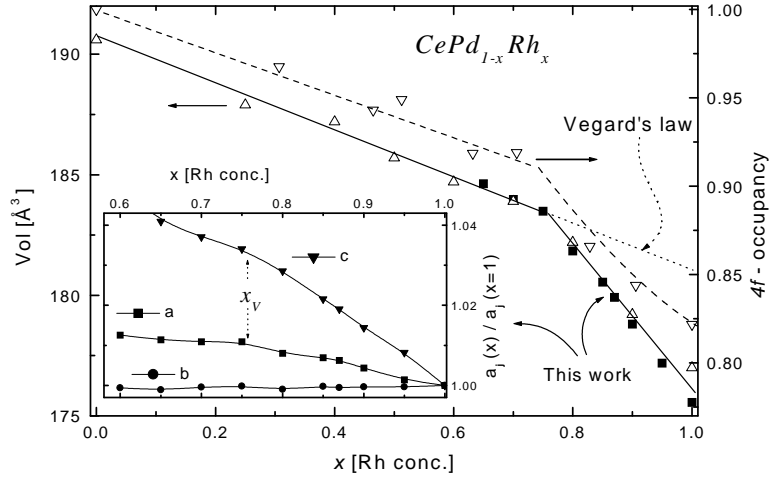


FIG. 1: Concentration dependence of the unit cell volume compared with data from Ref [14]. A clear deviation from Vegard's law occurs at  $x_V \approx 0.75$  at the onset of the valence instability, where also  $L_{III} - XAS$  spectroscopy indicates a stronger decrease of  $4f$  occupancy [14]. Inset: normalized variation of each lattice parameter ( $a_j$ ) showing the crystalline anisotropy of this system.

them.[6] In pure compounds (tuned by pressure) the F-GS is believed to end in a first order transition, disappearing at a classical critical point at finite temperature. On the contrary, some disorder introduced by alloying could smear out the first order phase transition, resulting in a continuous disappearance of magnetic order. [13] These predictions make F-alloys particularly interesting for the study of F-CP.

Among F-Ce compounds driven to non-magnetic state by doping Ce-ligands, the binary  $CePd_{1-x}Rh_x$  is one of the most suitable for this study. This system evolves from a  $F-Ce^{3+}$  state with  $T_C = 6.6K$  to a non-magnetic mixed-valence one, with susceptibility ( $\chi_{dc}$ ) and electrical resistivity ( $\rho$ ) maxima at  $T \approx 280K$ . [14] Its cell volume decreases continuously with  $x$  showing a deviation from Vegard's law around  $x_V = 0.75$ , while  $L_{III}-XAS$  measurements [14] indicate a significant decrease of the  $4f$  state occupancy beyond that concentration. Early studies [15] have extrapolated  $T_C(x) \rightarrow 0$  from  $T > 3K$  at  $T_C = 0$  for  $x \approx 0.65$ . However, recent studies performed at lower temperature revealed that  $T_C(x)$  does not tend to zero at the previously reported value because its negative curvature changes to slightly positive at  $x^* \approx 0.63$ . Consequently the  $T_C \rightarrow 0$  extrapolation was proposed at  $x_{cr} \approx 0.85$ . [16] Since the lowest transition temperature at  $T_C = 0.25K$  was observed for  $x = 0.80$ ,  $CePd_{1-x}Rh_x$  became one of the few systems, and the only F- one [17], in which  $T_C(x)$  was traced within more than one decade in temperature. These properties make  $CePd_{1-x}Rh_x$  an ideal candidate for the study of F quantum phase transitions.

## II. EXPERIMENTAL DETAILS AND RESULTS

A series of nine samples was prepared in the range  $0.6 \leq x \leq 1$  by arc melting the appropriate amount of pure elements under argon atmosphere. In order to ensure homogeneity, the resulting buttons were flipped over and remelted several times. For a further improvement of the homogeneity the buttons were melted again in a high frequency levitation crucible. At the end of this process the mass loss was found to be negligible (generally below 0.1%). The samples were then annealed for 7 days at  $700^\circ C$  in dynamic vacuum. Powder XR diffraction of crushed samples confirmed the orthorhombic CrB structure [18] and did not reveal sign of secondary phases. Since the Bragg peaks of the as crushed samples were rather broad, the powder used for the XR measurements was annealed at  $700^\circ C$  for 24 hrs in dynamic vacuum, leading to much narrower peaks. Using these sharp diffraction patterns we could determine precise values of the lattice parameters.

A standard SQUID magnetometer served for the determination of the magnetization from 2K up

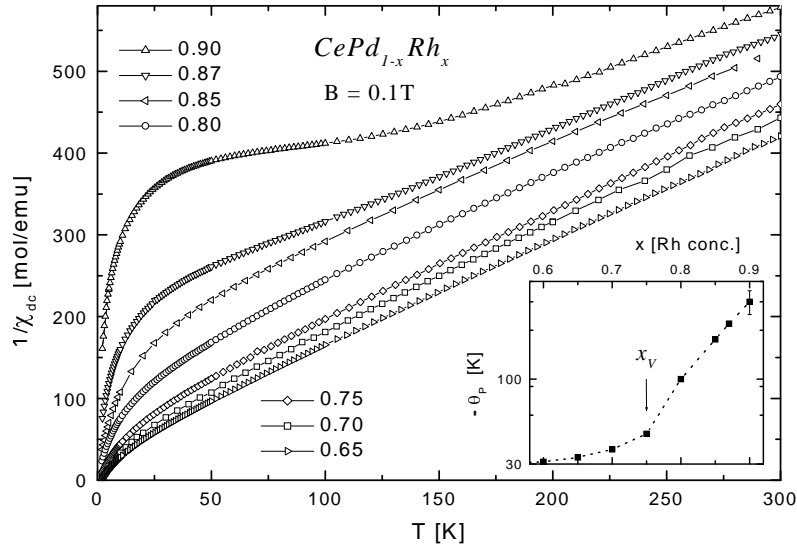


FIG. 2: Inverse dc-susceptibility as a function of temperature showing the increasing hybridization effects for  $x > 0.75$ . Inset: concentration dependence of Curie-Weiss temperature  $\theta_p$  in logarithmic scale, extrapolated from  $T \geq 100$  K ( $\geq 200$  K for  $x = 0.90$ ).

to room temperature in a 0.1 T magnetic field. The ac-susceptibility was measured using the mutual inductance technique, with a lock-in amplifier as detector working between 0.1 and 12.8 kHz with an excitation amplitude of  $\approx 10 \mu T$  in the  $0.5 \leq T \leq 6$  K range. For lower temperatures (i.e.  $18 \text{ mK} \leq T \leq 4$  K) a dilution refrigerator was used with the same excitation amplitude and frequencies between 13 Hz and 1113 Hz. The electrical resistivity was measured using a four probe dc-method in the temperature range from 0.5 K up to room temperature. Specific heat  $C_P(T)$  measurements on samples of about 1g were performed in a semi-adiabatic calorimeter at temperatures ranging from 0.5 K up to 20 K, using a heat pulse technique. Thermal expansion was measured along three perpendicular directions of polycrystals of rectangular shape  $\alpha_i$  with the aid of a ultra-high resolution capacitive dilatometer. The volume expansion coefficient  $\beta(T) = 1/V dV/dT$  is obtained from the sum of the linear expansion coefficients  $\beta = \alpha_1 + \alpha_2 + \alpha_3$ .

### A. High-temperature results

As mentioned before, the cell volume decreases continuously with increasing Rh content and the new measurements on intermediate concentrations allow to better establish the deviation from Vegard's law at  $x_V = 0.75$ , as shown in Fig.1. Because of the anisotropic crystalline structure of  $\text{CePd}_{1-x}\text{Rh}_x$ , we have analyzed the  $x$  dependence on each crystalline parameter. In the inset of Fig.1 one observes that the change of slope at  $x_V = 0.75$  occurs on "a" and "c" directions, while "b" remains practically unchanged. In order to confirm that such a deviation from Vegard's law corresponds to the onset of the valence instability, we include in Fig.1 the  $L_{III} - XAS$  results from Ref. [14]. These results coincide in the  $x_V$  determination as the concentration for the onset of the  $4f$  occupancy decrease.

DC-susceptibility ( $\chi_{dc}$ ), measured under an applied magnetic field of  $B=0.1\text{T}$ , were carried out on samples within the  $0.6 \leq x \leq 1$  concentration range. The temperature dependence between 2K and room temperature is depicted in Fig.2 as  $\chi_{dc}^{-1}$ . The high temperature ( $T > 100\text{K}$ ) dependence of samples  $0.65 \leq x \leq 0.87$  can be described by a typical Curie-Weiss (CW) law:  $\chi = C_c/(T - \theta_p)$ , with a negative  $\theta_p$  despite its F-GS (see inset of Fig.2). Beyond the critical concentration, it shows the features of a growing valence instability which dominates the signal CeRh (c.f.  $x = 1$ ), with a broad maximum centered at  $\approx 240$  K (not shown). As it occurs in systems undergoing a magnetic to mixed valence transition, the molecular field (represented by  $\theta_p$ ) is overcome by the Kondo effect. For that case a  $\chi = C_c/(T + 2T_K)$  expression was proposed [19] where  $T_K$  is the Kondo temperature reflecting the  $J_K$  increase since  $T_K \propto 1/\delta J_K$ . [8]

The crystalline electrical field (CEF) effect can be observed in  $x = 0.70$  with  $\chi_{dc}(T)$  plotted as a

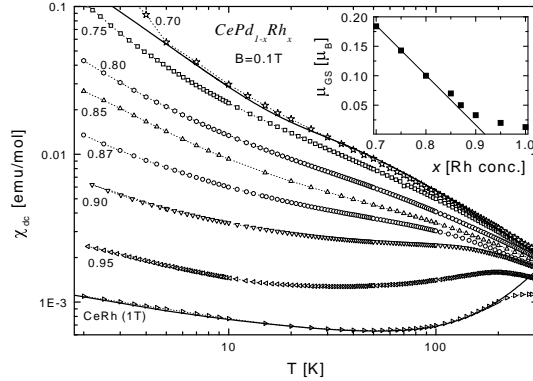


FIG. 3: Temperature dependence of dc-susceptibility in a double logarithmic representation, showing the effect of hybridization on the excited CEF levels at high temperature and the weakening of the effective moments at low temperature. Continuous curves are fits for  $x = 0.70$  and  $x = 1$  data using eq(1) and eq.(2) respectively.

function of temperature in Fig.3, in a double logarithmic representation. To evaluate the energy of the first excited level ( $\Delta_{CF}$ ) we used a simplified formula applicable to the low temperature range (i.e.  $T < \Delta_{CF}$ ):

$$\chi(T)_{CF} = \mu_{GS}^2 + \mu_{CF}^2 \times \exp(-\Delta_{CF}/T)/(Z \times T) \quad (1)$$

where  $\mu_{GS}$  ( $\mu_{CF}$ ) is the ground (excited) state effective moment and  $Z$  the partition function. Using this simple equation we obtain  $\Delta_{CF} \approx 55K$  and the respective effective moments:  $\mu_{GS} \approx 0.18\mu_B$  and  $\mu_{CF} \approx 0.34\mu_B$  (see continuous curve on  $x = 0.70$  in Fig.3). The strong increase of the  $\chi_{dc}$  below 4K is due to the onset of ferromagnetic correlations. The progressive weakening of  $\mu_{GS}(x)$  evaluated around 2K is depicted in the inset of Fig.3. The  $\mu_{GS}$  points between  $0.70 < x < 0.80$  extrapolate to zero at  $x \approx 0.90$ , whereas the deviation from such extrapolation for  $x \geq 0.90$  can be related to remnant low energy excitations observed in  $C_m/T$  measurements to be discussed below.

On the non-magnetic limit, CeRh shows the typical behavior for a mixed valence (MV) compound plus a power law increase at low temperature:

$$\chi(T) = \chi_0 + bT^2 + c/T^q \quad (2)$$

The Pauli-type contribution is  $\chi_0 = 0.46 \times 10^{-3}$  emu/mol and the  $bT^2$  dependence reflects the presence of spin fluctuations, in this case with  $b = 0.12 \times 10^{-3}$  emu/molK<sup>2</sup>. The increase of  $\chi(T)$  below about 30K indicates a reminiscence of magnetic moments even at the CeRh limit. This magnetic contribution cannot be attributed to magnetic impurities only because its temperature dependence:  $c/T^q \propto T^{-0.45}$  does not correspond to a Curie-Weiss law.  $M$  vs  $B$  measurements at  $T=2K$  and up to  $B=5T$  (not shown) indicate that only a small magnetic contribution, which saturates at  $B \approx 3T$  is due to impurities. For this compound the Wilson ratio,  $\chi_0/\gamma_0 = 0.036$  emuK/mol corresponds to the expected value for an MV (i.e. six fold degenerated) ground state [7]. Once normalized:  $R = (\pi k_B/\mu_{eff})^2 \chi_0/\gamma_0 = 1 + 1/2J = 1.2$ , since for Ce-MV systems  $J = 5/2$ . [20]

The electrical resistivity ( $\rho$ ) measured up to room temperature of the samples within the  $0.80 < x < 1$  Rh concentration is displayed in Fig.4. There, our results on the  $x = 0.80$  and 1 samples are compared with those of  $x = 0.85$  and 0.90 (after Ref.[14]) once normalized to their respective values at room temperature. Two features characterize  $\rho(T)$ , one is the rapid increase of the hybridization effect on the high temperature electronic scattering and the other the drastic drop of the residual resistivity ( $\rho_0$ ) as  $x \rightarrow 1$ . The former is concomitant with the increase of  $\theta_P$  ( $\propto T_K$ ) in that concentration range. In the case of  $x = 0.80$  a  $\rho(T)$  upturn occurs below 10K (see upper inset in Fig.4). Such an electronic scattering arises nearly two decades above the  $\chi'_{ac}$  cusp and thermal expansion minimum (at  $T = 0.25K$ ) and is probably due to magnetic correlations related to that transition. The lower inset in Fig.4 shows the analyzed  $\Delta\rho \propto T^2$  dependence up to  $\approx 40K$ . The weak upturn observed at low temperature will be analyzed in the context of other low temperature properties.

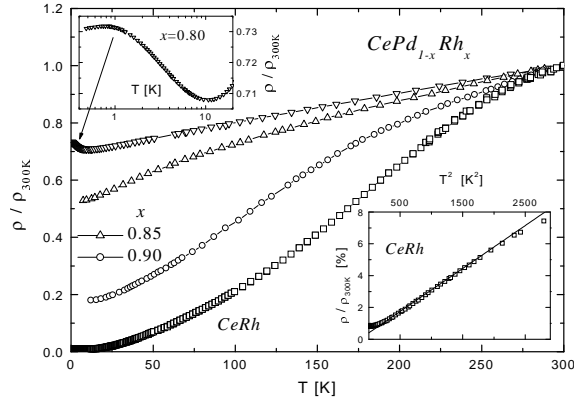


FIG. 4: Electrical resistivity normalized at room temperature showing the rapid decrease of the low temperature scattering above  $x_{cr}$  and the increase of hybridization effect with the valence instability. Upper inset: detail of the merging magnetic scattering in the  $x = 0.80$  sample. Lower inset: detail of the  $\rho \propto T^2$  dependence of CeRh up to 40K and the slight upturn below 15K.

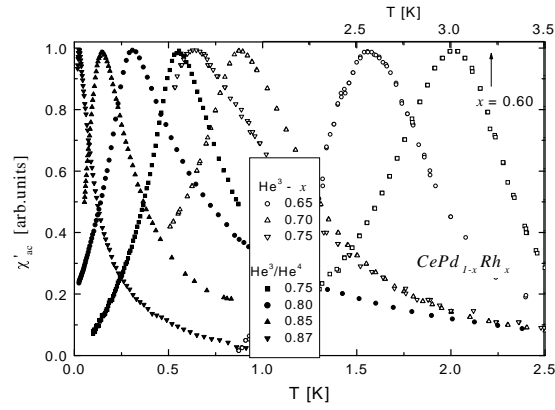


FIG. 5: Inductive signal of ac-susceptibility,  $\chi'_{ac}$ , normalized at their respective maximum values. For clarity, the temperature dependence of sample  $x = 0.60$  (only) is depicted on the upper abscissa of the figure.

## B. Low temperature results

In order to determine  $T_C(x)$  below the lowest value previously reported ( $T_C = 3\text{ K}$  [15]), we have performed two sets of  $\chi_{ac}$  measurements, one down to 0.5K in a  $\text{He}^3$  cryostat and the other down to 20mK in a dilution refrigerator. The F-phase boundary was traced following the temperature of the maximum of the inductive signal  $\chi'_{ac}(T)$  in the  $0.60 \leq x \leq 0.90$  samples. These results are presented in Fig.5, after normalizing the measured signal with their values at 5K and the respective maxima. The sharpness of the anomaly (not depending on  $x$ ) also indicates that eventual atomic disorder introduced by Pd/Rh substitution does not affect the F-transition, which keeps its shape down to the critical concentration ( $x_{cr}$ ).

The electronic contribution to the specific heat ( $C_{el}$ ) was obtained by subtracting the phonon contribution ( $C_{ph}$ ) to measured values ( $C_P$ ) as:  $C_{el} = C_P - C_{ph}$ . The stoichiometric compound LaRh was taken as the reference for the  $C_{ph}$  determination. Fig.6 collects the  $C_{el}/T$  results. Though the specific heat magnetic anomaly ( $C_m$ ) dominates  $C_{el}$  at the F-phase, the experimental data indicate that with increasing  $x$  a Fermi liquid (FL) contribution,  $\gamma(x)$ , arising from the MV component, becomes important and then  $C_{el}/T$  has to be accounted as  $C_{el}/T = C_m/T + \gamma$  for high Rh concentration. It can be seen in Fig.6 that sample  $x = 0.50$  still shows a sharp transition that broadens for  $x \geq 0.60$  (i.e. for  $x \geq x^*$ ). However, the maximum of  $C_{el}/T$  stops decreasing and becomes nearly constant for the  $x = 0.60, 0.65$  and  $0.70$  samples, like in other Ce-systems tuned to their quantum critical points (QCP).[21] Beyond  $x_{cr}$  the  $\gamma$  component tends to dominate the total contribution and,

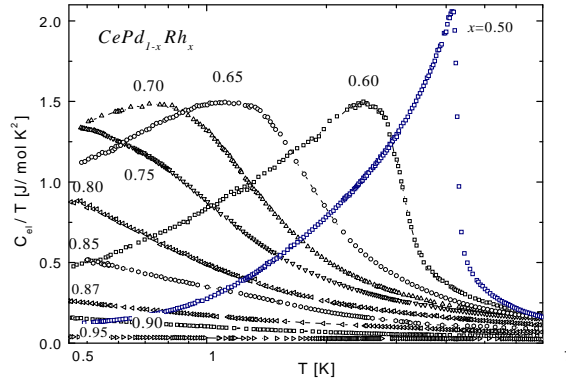


FIG. 6: Total electronic contribution to the specific heat divided temperature as a function of temperature in a logarithmic scale for samples around the critical region.

samples  $x = 0.90, 0.95$  and  $1$ , the FL contribution is found to be  $\gamma = 0.047, 0.028$  and  $0.017 \text{ J/mol K}^2$  respectively. This type of contribution was observed in many Ce-systems at the onset of their valence instabilities.[9] A detailed analysis on the temperature dependence of  $C_{el}(T)/T$  around  $x_{cr}$  is made in Fig.7. There, a logarithmic temperature dependence is observed for  $x = 0.80$  and  $0.85$  samples (see Fig.7a), whereas  $x = 0.87, 0.90$  and  $0.95$  show a power law  $T$  dependence as proved by the double logarithmic representation in Fig.7b. These results are described by a  $C_m/T = AT^{-q}$  formula with the exponent  $q = 0.54 \pm 0.01$  and  $A = 0.173, 0.102$  and  $0.012 \text{ J/mol K}^{2-q}$  respectively. In the case of sample  $x = 0.95$ , the  $\gamma(x)$  contribution was subtracted since  $C_m(T)/T$  becomes very small at this Rh concentration.

Thermal expansion measurements performed down to  $T \approx 0.1 \text{ K}$  on samples  $0.80 \leq x \leq 0.90$  are shown in Fig.8. The magnetic transition in the  $x = 0.80$  alloy is clearly identified by a minimum at  $0.25 \text{ K}$ , in coincidence with the  $\chi'(T)$  measurements. Noteworthy is the change of sign of  $\beta$  at  $x = 0.85$  in coincidence with the already mentioned changes in other experimental parameters. Nevertheless, it has to be mentioned that in this sample there is still a positive contribution observed in one of the measured directions. The anisotropic expansion of this system has to be related with the intrinsic crystalline anisotropy. Detailed analysis of the non-Fermi liquid behavior of  $\beta(T)$  will be presented elsewhere and compared with that of  $C_m(T)$ .

### III. DISCUSSION

The competition between the vanishing F- order and the growing Kondo screening with Rh concentration is visualized in the magnetic phase diagram in Fig.9. There one appreciates that, instead of a continuous negative curvature in  $T_C(x)$ , an inflection in the phase boundary occurs at  $x^* = 0.65$ . The characteristic of this concentration is that  $T_K(x)$  (considered proportional to  $\theta_P(x)$ [19]) starts to increase as shown on the right side of Fig.9 in a logarithmic scale. Though Doniachs model includes both magnetic and Kondo interactions, it predicts a vanishing  $T_C(x)$  without any possible change of curvature. In order to discuss such a case we have to take into account that two critical behaviors occur at similar concentration as it is indicated by high and low temperature measurements. One concerns the valence instability signed by the deviation from Vegard's law and  $4f$  occupation reduction at  $x \geq x_v$  and the other the magnetic critical point at  $x_{cr} \approx 0.87$ . Though this peculiar situation was already observed in a few Ce-systems, [9] it was never studied in detail before. In fact, the present investigation demonstrates that the previous  $T_C \rightarrow 0$  extrapolation to  $x \approx 0.65$  [14] did not account for the change of curvature occurring at  $x^* = 0.60$  that originates an extended "tail" at low temperatures. Besides the change of curvature there are other clear indications for significant modifications in the GS properties between  $x^*$  and  $x_{cr}$ .

As mentioned before, the well defined  $C_m/T(T_C)$  jump at  $x = 0.50$  broadens for  $x = 0.60$ , keeping a similar relative width and the same maximum value up to  $x = 0.70$ . Since no sudden changes in the atomic order are expected between  $x = 0.50$  and  $0.60$ , this modification confirms the changes occurring around  $x^*$ . At higher Rh concentration (c.f.  $0.80$ ) the  $C_m/T(T)$  dependence becomes logarithmic in

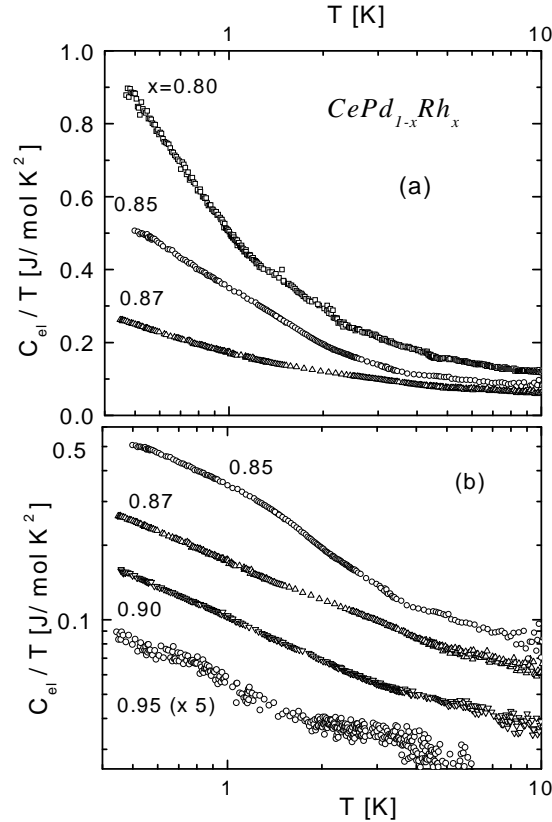


FIG. 7: a) Specific heat divided temperature showing the logarithmic dependence on  $T$  at low temperature on the critical concentration. b) Double logarithmic representation showing the power law temperature dependence beyond the critical concentration. For sample  $x = 0.95$ , the  $\gamma=0.028\text{J/molK}^2$  contribution is subtracted (see the text). Notice that data from samples  $x = 0.85$  and  $0.87$  are also included in panels b) and a) respectively for comparison.

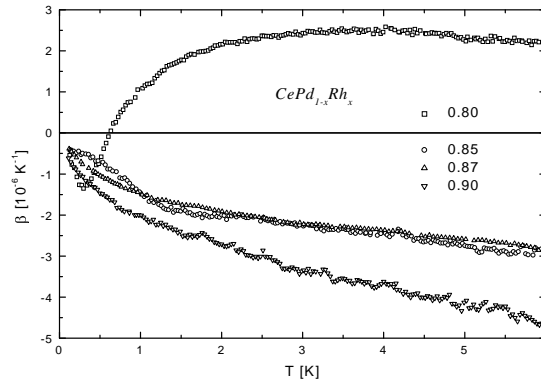


FIG. 8: Thermal expansion measurements showing  $T_C$  at 0.25K and the sudden change of sign at  $x = 0.85$ .

agreement with theoretical predictions for 3-dimensional itinerant ferromagnets.[22] Coincidentally, the  $\chi_{ac}$  maximum starts show frequency ( $\omega$ ) dependence for  $x \geq 0.70$ . These features are usually associated to atomic disorder in diluted systems. However, due to the *lattice* character of the magnetic atoms and the similar atomic size of Ce ligands (c.f. Pd and Rh) a sudden appearance of a spin glass like behavior between  $x = 0.60$  and  $0.70$  is unlikely. Nevertheless, in an ample concept of disorder, the presence of random distribution of interactions competing in certain ranges of energy have to be

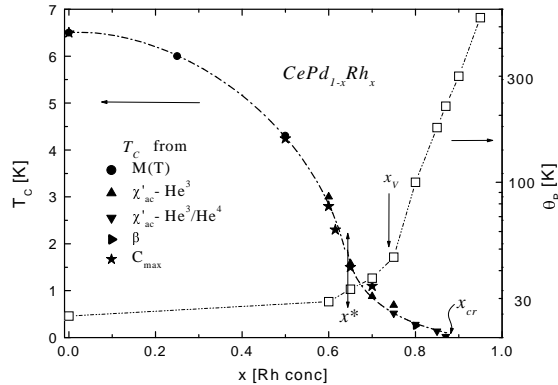


FIG. 9: Magnetic phase diagram along the full concentration range, extracted from magnetic ( $M, \chi'_{ac}$ ) and thermal ( $\beta, C_m/T|_{max}$ ) properties.  $x^*$  marks the inflection of  $T_C(x)$  curvature,  $x_V$  the onset of the valence instability and  $x_{cr}$  the critical point. The concentration dependence of the Curie-Weiss temperature is included for comparison in a logarithmic scale (on the right axis) to show its rapid increase for  $x > x_V$ .  $\Delta_{CF}$  indicates the estimated first CEF splitting. Dash-dot lines are guides to the eye.

taken into account. Magnetic ( $J_R$ ) and Kondo ( $J_K$ ) interactions, powered by respective Pd and Rh Ce-neighbors with random spacial distribution, are expected to build up an inhomogeneous pattern for those parameters. Since in such a scenario no more long range F-order is expected, for  $x > x^*$  we will identify the line of  $\chi_{ac}$  maxima as  $T_C^*(x)$ .

It was shown that random hybridization ( $\propto J_K(x)$ ) leads to a finite probability of very small  $T_K$  values ( $T_K^L$ ) and to non-Fermi-liquid behavior.[23] This may explain that a magnetic character of the GS may coexist with a strong increase of  $T_K(x > x_V)$ . On the other hand, spin disordered systems close to their QCP were described as Griffiths phases due to the possible formation of non percolating magnetic clusters.[24] Since this scenario predicts a power law  $C_m(T)$  dependence, for our case it only applies to the  $x \geq x_{cr}$  region. A more realistic description can be done accounting for an inhomogeneous distribution of each Ce environment, where  $J_R(x)$  and  $J_K(x)$  act simultaneously.[25]

The strong anisotropy of this system is also expected to play a role in the coexistence between the magnetic GS and the strongly hybridized excited CEF levels wave functions. The orthogonality of the CEF levels wave functions leads to the possibility of different intensities between local and conduction spin couplings due to their different mixing matrix elements. Such a situation becomes sensitive when  $T_K \approx \Delta_{CF}$  since the broadening of the excited CEF levels increase their influence on the low energy range.

The actual hybridization effect (given by  $T_K^L$ ) on the low-lying levels can be evaluated by means of a low temperature property like the magnetic entropy ( $S_m(x, T)$ ). Taking profit that  $S_m \propto 1/T_K$  [26], one can obtain  $T_K^L(x)$  from the measured  $S_m$  at a fixed temperature. In this case, we have extracted  $S_m$  at  $T = 8K$  from the  $S_m(T)$  data shown in Fig.10 and computed the  $RLn2/S_m(x)$  values as depicted in the inset of Fig.10. Though on the Rh rich side its tendency is similar to the extracted form  $\theta_P(x)$ , a clear deviation between those parameters is observed between  $x_V$  and  $x_{cr}$  since the GS and the CEF excited levels are differently affected. Further increase of  $J_K(x)$  leads to the collapse of the CEF effect and the sixfold degenerated Hund's rule GS takes over at the MV limit.

The change of sign in the thermal expansion indicates that the volume behaves completely different on both sides of the critical concentration. Starting from  $T = 0$ , sample  $x = 0.80$  first contracts to undergo the magnetic transition, but then rapidly expands. On the contrary, for  $x \geq 0.85$  (i.e.  $x_{cr}$ ), the volume continuously contracts (at least up to 6K). Even being anisotropic, the negative sign of  $\beta(T)$  for  $x \geq 0.85$  is quite surprising because in that concentration range the MV regime becomes dominant. In fact, well known Ce-MV compounds show positive  $\beta(T)$  coefficient (e.g. CeSn<sub>3</sub> [27]) because the main energy scale, related to  $T_K$ , increases under pressure. However, since this observation corresponds to the low temperature range (i.e. up to 6K  $\ll T_K$ ) it only involves the low energy excitations of the system, where a diverging  $C_m/T$  component is still present. Taking profit that the linear thermal expansion of each sample was measured in three perpendicular directions, further information about anisotropic effects of this system can be extracted. Notably, only in one direction  $\alpha(T)$  is positive (arbitrarily label as  $\alpha_1$ ) and becomes zero at  $x = 0.87$ , whereas the other



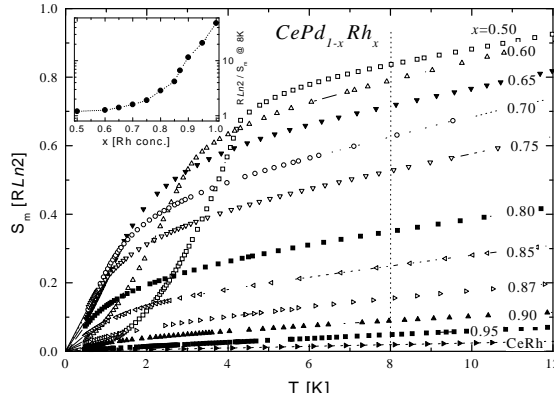


FIG. 10: Entropy gain on temperature for all studied samples, normalized to  $RLn2$ . Inset: inverse of entropy at fixed temperature (8K) as a function of concentration (see the text).

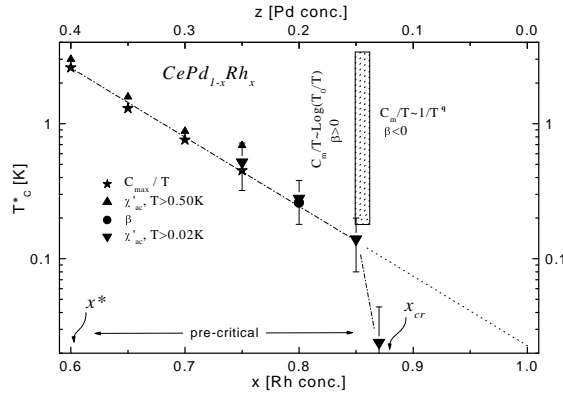


FIG. 11:  $T_C^*(x)$  dependence at the pre-critical concentration showing its logarithmic decrease and its sudden disappearance of the  $\chi'_{ac}(T)$  cusp. The change of thermal properties is indicated around the critical concentration.

( $\alpha_2$  and  $\alpha_3$ ) show an increasing negative temperature dependence. Further measurements on single crystals are certainly required to relate this anisotropic behavior to the actual crystalline axis, see Ref.[28]

In Fig.11 we show a detailed  $T_C^*(x)$  dependence obtained from the different techniques, notably  $\chi'_{ac}$  at very low temperature, which are depicted in a logarithmic scale. The positive curved "tail", already presented in the phase diagram of Fig.9, can be described by a simple function:

$$T_C^*(z) = 0.022 K \times e^{12z} \quad (3)$$

where  $z = 1 - x$  corresponds to Pd concentration. This permutation of the concentration parameters dependence is not a minor detail since it indicates that the  $T_C^*(z)$  evolution refers to a *smearred* phase transition [29] even beyond the CeRh limit, in agreement with the remnant contribution of  $C_m/T$  on that side of the phase diagram. Since this description is valid for  $z > 0.13$ , it seems that some type of *percolation* between magnetic *rare* regions [2] is needed to produce the cusp detected by  $\chi_{ac}$ . Such a *percolation* threshold is in agreement with the onset of the power law dependence of  $C_m/T$  since, as mentioned before, the formation of Griffiths phases requires the existence of non-percolating clusters, that occurs for  $x > 0.87$ . The fact that the  $T_C^*$  variation can be described by such a simple  $z$  dependence suggests that the physics at the *pre-critical* region is governed by a critical behavior lying beyond the CeRh limit. This pattern implies a split of the phase diagram description at  $x \approx x^*$ , which seems to present two distinct regions, represented by the  $T_C$  boundary and the  $T_C^*$  line respectively. On the canonical F- (Pd rich side c.f.  $0 \leq x \leq x^*$ ) the  $T_C(x)$  phase boundary (between  $6K \geq T_C > 2K$ ) points to the former [15] critical point at  $x \approx 0.65$ . Beyond  $x^*$  (i.e. below about 2K) another type of

criticality dominates the scenario according to the drastic changes in the low temperature properties. The question arises whether this threshold is governed by the concentration (i.e. chemical potential) or by the exhausting thermal fluctuations overcome by quantum fluctuations.

Such a *thermal* threshold is not an arbitrary proposition since other well known AF-Ce systems show similar changes in their magnetic phase boundaries at that temperature (c.f. thermal energy) even close to a first order transition, like:  $\text{CeIn}_{3-x}\text{Sn}_x$  with  $x^* \approx 0.40$ , where  $T_N = 2\text{ K}$ , [21] and  $\text{CeCu}_2(\text{Si}_{1-z}\text{Ge}_z)_2$  with  $z^* = 0.25$  K and also  $T_N = 2\text{ K}$  [30]. Notice that parameters "x" and "z" are used like in the present context, i.e.  $x \rightarrow 1$  ( $z \rightarrow 0$ ) is the non-magnetic side.

Going back to Rh concentration  $x$  as the control parameter, another important observation is the frequency ( $\omega$ ) dependence of the  $\chi'_{ac}$  cusp. Such a dependence is only observed within  $0.70 \leq x \leq 0.87$  and the question arises whether it is due to a canonical spin-glass behavior or to fluctuations related to the QCP. Since a  $C_m/T \propto -\log(T/T_0)$  dependence is predicted for a Non-Fermi-Liquid behavior (instead of the  $\propto 1/T^2$  for a spin-glass), quantum critical fluctuations may be the responsible such a  $\chi'_{ac}(\omega)$  dependence.[31] Nevertheless, other hallmarks of spin-glass GS, like the difference between zero-field and field-cooling or the time dependence of  $\chi'_{ac}$  response under field suppression have to be explored.

#### IV. CONCLUSIONS

The phase diagram of F-  $\text{CePd}_{1-x}\text{Rh}_x$  was traced between  $T_{C,x=0} = 6\text{ K}$  and  $T_{C,x=0.87}^* \approx 20\text{ mK}$ . Three characteristic concentrations were identified:  $x^* \approx 0.65$ ;  $x_V \approx 0.75$  and  $x_{cr} \approx 0.87$ . The former marks the cross over from a classical phase boundary (with a negative curvature) into a positive curved "tail" which ends at  $x_{cr} = 0.87$ . In that region a frequency dependence of the  $\chi'_{ac}$  cusp is also detected.

Independently from this magnetic GS, a deviation from Vegard's law occurs at  $x_V$ , indicating the onset of the valence instability. Beyond that concentration  $T_K(x)$  increases exponentially. Unlike typical AF systems, where  $x_V > x_{cr}$ , this ferromagnet has its critical concentration ( $x_{cr} \approx 0.87$ ) above the onset of the valence instability and therefore  $x_V < x_{cr}$ . Such a characteristic inhibits the appearance of HF behavior because at that concentration  $J_K$  is already largely developed, leading to the broadening of the quasi-particles band with the consequent reduction of their effective mass. Besides this  $\gamma(x)$  decrease, there is a remanence of low laying magnetic excitations accounted by the  $C_m/T \propto 1/T^q$  contribution. Such a coexistence of magnetism with highly hybridized quasi-particles occurs in an inhomogeneous distribution of  $J_R$  and  $J_K$  couplings produced by the random distribution of Pd and Rh Ce-ligands.

The different magnetic behavior observed between high and low temperature properties of this system is related to its strong anisotropic character. Such anisotropy is clearly observed in the crystalline parameters and in thermal expansion measurements. Therefore a different degree of hybridization occurs between the ground and the excited CEF levels.

The outstanding findings around  $x_{cr}$  are the change temperature dependence of  $C_m/T$ , from logarithmic to power law coincident with the change of sign of  $\beta$ . Notably, around that concentration  $C_m/T$  and  $\chi_{dc}$  coincide in their  $T^{-q}$  temperature dependence. Though in the pre-critical ( $x^* < x < x_{cr}$ ) region, the logarithmic  $C_m/T(T)$  dependence is in agreement with the theoretical predictions for 3-dimensional itinerant ferromagnets, its transformation to a power law beyond  $x_{cr}$  indicates that a sort of percolation between "rare" regions can play an important role in this behavior. The simultaneous effect of ferromagnetic and valence fluctuations may result in a more complex scenario for the electronic scattering, which is not accounted in the model.

Finally, we have shown that a better understanding of the phase diagram can be achieved by splitting it into two regions. One with the long range F-order extrapolating  $T_C(x) \rightarrow 0$  at  $\approx 0.65$  and the other (below about 2K) extrapolating  $T_C^*(x)$  beyond the CeRh limit. Altogether,  $\text{CePd}_{1-x}\text{Rh}_x$  has proved to be an exemplary system for studying the influence of doping on the quantum criticality in a Ferromagnetic environment, covering two and a half decades of temperature.

### Acknowledgments

This work was partially supported by F. Antorchas - DAAD cooperation program (proj. # 14248/7). J.G.S. is member of the CONICET and Instituto Balseiro of Argentina.

- 
- [1] See e.g. Proceedings of SCES'04: Physica B **359-361** (2005) and SCES'05 (to be published).
  - [2] T. Vojta, Ann.Phys. (Leipzig) **9** (2000) 403 and P. Coleman, A. Schofield, Nature **433** (2005) 225.
  - [3] G.R Stewart, Rev. Mod. Phys. **73** 797 (2001).
  - [4] see for example: S.M. Evans, A.K. Bhattacharjee and B. Coqblin; Physica B **171** (1991) 293.
  - [5] M. Uhlarz, C. Pfeiderer, S.M. Hayden, Phys. Rev. Lett. **93** (2004) 256404.
  - [6] T.R. Kirkpatrick and D. Belitz, Phys. Rev. B **67** (2003) 024419.
  - [7] J.G. Sereni, *Handbook for Physics and Chemistry of Rare Earths*, edited by K.A. Gschneidner Jr. and L. Eyring, Chap. 98, Vol 15 ( Elsevier Science B.V, 1991).
  - [8] S. Doniach, Physica B **91**, 231 (1977) and M. Lavagna, C. Lacroix, and M. Cyrot, Phys. Lett. **90A**, 210 (1982).
  - [9] J. G. Sereni, Physica B **215**, 273 (1995), and references therein.
  - [10] B. Coqblin, J. Arispe, J. R. Iglesias, C. Lacroix, and K. Le Hur, J. Phys. Soc. Japan **65**, Suppl. B, 64 (1996).
  - [11] S. Sülow, M.C. Aronson, B.D. Rainford and P.Haen, Phys. Rev. B **82** (1999) 2963.
  - [12] T. Burghardt, A. Eichler, S. Sülow and J. A. Mydosh, Physica B **259-261** (1999) 99.
  - [13] T. Vojta, Phys. Rev. Lett. **90** (2003) 107202.
  - [14] J.P. Kappler, M.J. Besnus, A. Herr, A. Meyer and J. Sereni, Physica B **171** (1991) 346.
  - [15] J.G. Sereni, E. Beaurepaire and J.P. Kappler, Phys. Rev. B **48** (1993) 3747.
  - [16] J.G. Sereni, R. Küchler and C. Geibel, Physica B **359-361** (2005) 41.
  - [17] J.G. Sereni, J. Phys. Soc. Japan **70** (2001) 2139.
  - [18] D. Hohnke and E. Parthé, Acta Cryst. **20** (1966) 572.
  - [19] H.R. Krishna-murthy, K.G. Wilson and J.W. Wilkins, Phys. Rev. Lett. **35** (1975) 1101.
  - [20] see for example; M.J. Besnus, J.P. Kappler and A. Meyer, Physica **130B** (1985) 127. Notice that in the case of HF (with doublet GS)  $J = 1/2$  and then  $R = 1 + 1/2J = 2$ .
  - [21] P. Pedrazzini, M. G-Berisso, N. C-Canales, M. Deppe, C. Geibel and J.G. Sereni, Eur.Phys.J. **B38** (2004) 445.
  - [22] L.B. Ioffe and A.J. Millis; Phys. Rev. B **51** (1995) 16151.
  - [23] E. Miranda, V. Dobrosavljevic and G. Kotliar, Phys. Rev. Lett. **78** (1997) 290.
  - [24] A.H. Castro-Neto, G. Castilla and B.A. Jones, Phys. Rev. Lett. **81** (1998) 3531.
  - [25] A.M. Lobos, A.A. Aligia and J.G. Sereni, Eur. Phys. J. B **41** (2004) 289.
  - [26] H.-U. Desgranges and K.D. Schotte, Phys. Lett. **91A** (1982) 240.
  - [27] see for example J.G. Sereni, J. Phys. F: Metal Phys. **10** (1980) 2831.
  - [28] M. Deppe, P. Pedrazzini, N. Caroca-Canales, C. Geibel, J.G. Sereni, Physica B (2005), to be published.
  - [29] for a "Smearred quantum phase transition" description see: R. Sknepnek and T. Vojta, Phys. Rev. B **69** (2004) 174410.
  - [30] O. Stockert, M. Deppe, E. Faulhaber, H.S. Jeevan, R. Schneider, N. Stuesser, C. Geibel, M. Lövhaupt and F. Steglich, Physica B **359-361** (2005) 349.
  - [31] D.R. Grempel and M.J. Rozenberg, Phys. Rev. B **60** (1999) 4702.